ACS APPLIED MATERIALS & INTERFACES

Research Article

www.acsami.org

Early Assessment and Correlations of Nanoclay's Toxicity to Their Physical and Chemical Properties

Alixandra Wagner,[†] Andrew P. White,[†] Todd A. Stueckle,[‡] Derrick Banerjee,[§] Konstantinos A. Sierros,[§] Yon Rojanasakul,[∥] Sushant Agarwal,[†] Rakesh K. Gupta,[†] and Cerasela Zoica Dinu*[,†]

[†]Department of Chemical and Biomedical Engineering, West Virginia University, Morgantown, West Virginia 26506, United States

[‡]Health Effects Laboratory Division, National Institute for Occupational Safety and Health, Morgantown, West Virginia 26505, United States

[§]Department of Mechanical and Aerospace Engineering, West Virginia University, Morgantown, West Virginia 26506, United States

[∥]Department of Basic Pharmaceutical Sciences, West Virginia University, Morgantown, West Virginia 26506, United States

Supporting Information

ABSTRACT: Nanoclays' functionalization with organic modifiers increases their individual barrier properties, thermal stability, and mechanical properties and allows for ease of implementation in food packaging materials or medical devices. Previous reports have shown that, while organic modifiers integration between the layered mineral silicates leads to nanoclays with different degrees of hydrophobicity that become easily miscible in polymers, they could also pose possible effects at inhalation or ingestion routes of exposure. Through a systematic analysis of three organically modified and one pristine nanoclay, we aimed to relate for the first time the physical and chemical characteristics, determined via microscopical and spectroscopical techniques, with the potential of these nanoclays to induce deleterious effects in in vitro cellular systems, i.e. in immortalized and primary human lung epithelial cell lines. To derive information on how functionalization could lead to toxicological profiles throughout nanoclays' life cycle, both as-received and thermally degraded nanoclays were evaluated. Our analysis showed that the organic modifiers chemical composition influenced both the physical and chemical characteristics of the nanoclays as well as their toxicity. Overall, when cells were exposed to nanoclays with organic modifiers containing bioreactive groups, they displayed lower cellular numbers as well more elongated cellular morphologies relative to the pristine nanoclay and the nanoclay containing a modifier with long carbon chains. Additionally, thermal degradation caused loss of the organic modifiers as well as changes in size and shape of the nanoclays, which led to changes in toxicity upon exposure to our model cellular systems. Our study provides insight into the synergistic effects of chemical composition, size, and shape of the nanoclays and their toxicological profiles in conditions that mimic exposure in manufacturing and disposal environments, respectively, and can help aid in safe-by-design manufacturing of nanoclays with user-controlled functionalization and lower toxicity levels when food packaging applications are considered.

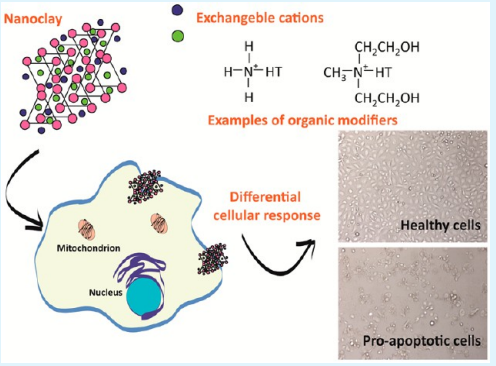

KEYWORDS: *nanoclay, toxicity, human lung epithelial cell, life cycle, organic modifier, safe-by-design manufacturing*

1. INTRODUCTION

With an estimated growth rate of about 25% annually,[1] nanocomposites or composites containing nanoclays incorporated into polymers are expected to have wide implementation in commercial and industrial products,[2] from food packaging materials[3] to automotive[4] and medical devices.[5] In food packaging, for instance, nanoclays are organically modified to allow for better exfoliation within the polymer matrix[4] at a low silicate weight percent,[6] leading to commercial applications of almost 70% of the market volume.[7] The organic modification generally occurs via an ion exchange reaction with the positively charged ions present between the nanoclay platelets[4] and directly impacts the type of polymer in which the nanoclay can be exfoliated as well as the properties of the resulting nanocomposite. The increased implementation of nanoclays is a result of the improved mechanical strength,[8] barrier properties,[8] UV dispersion,[9] and fire resistance[10] that they inflict to the polymeric packaging materials, thus reducing gas and moisture permeability,[11] allowing for a longer shelf life[4] while still producing a lightweight,[12] transparent[13] material capable of withstanding physical manipulation[12] and other environmental elements such as light and heat.[12]

Some of the most common nanoclays used in food packaging are Nanomer I.31PS, Nanomer I.34TCN, and Nanomer I.44P. These nanoclays, belonging to the montmorillonite (MMT) clay family, are made up of 2:1 phyllosilicates consisting of

Received: May 11, 2017
Accepted: August 11, 2017
Published: August 11, 2017

DOI: 10.1021/acsami.7b06657
ACS Appl. Mater. Interfaces 2017, 9, 32323−32335

2 silicate−oxygen tetrahedral sheets bounding an aluminum octahedral sheet[14] with each of the nanoclays containing a different organic modifier that tailors its name as well as its exfoliation ability in the specific types of polymer matrixes.[12] Specifically, Nanomer I.31PS is modified with aminopropyltriethoxysilane and octadecylamine, while Nanomer I.34TCN and Nanomer I.44P are modified with methyl dihdroxyethyl hydrogenated tallow ammonium and dimethyl dialkyl amine, respectively. Previous results showed that upon such modifications, Nanomer I.31PS and Nanomer I.44P can be exfoliated in polyethylene[15] and polypropylene[16] to result in composites with increased Young's[15,17] and storage moduli,[15] thermal stability,[17] and tensile strengths,[17] which ensures enhanced shelf life of food packaging products. Further, addition of Nanomer I.34TCN into polylactic acid[18,13] has resulted in nanocomposites with increased barrier properties,[18,13] thermal stability,[18] and tensile modulus[18] along with high transparency,[13] thus making Nanomer I.34TCN a good candidate for the green food packaging area, i.e., using biodegradable polymers from renewable resources to allow for a more environmental friendly food packaging material formation.

Previous reports also showed that manufacturing and disposal of nanocomposites used in food packaging applications could possibly lead to nanoclays being released from their polymer matrix,[19,20] which can pose health concerns if the exposure is via inhalation or ingestion routes. General in vitro assessment has found that both pristine and organically modified nanoclays cause decreased cellular proliferation,[21] mitochondrial damage,[22] reactive oxygen species (ROS) generation,[22] membrane[22] and DNA damage,[23] micronuclei induction,[24] and changes in mRNA expression[24] in lung epithelial cells,[21,25] liver cells,[22] colon cells,[23] or skin cells,[25] with the degree of toxicity dependent on the cell type, dosage, and the organic modifier itself. Additionally, in vivo results revealed significant toxic effects through alteration of protein expressions after organically modified nanoclay was administered orally to rats[26] as well as robust inflammatory responses characterized by transient neutrophilia, for instance.[27]

However, while such reports hint at varying degrees of toxicity, minimal information is available to compare and contrast the effects of the unique physicochemical properties of the nanoclays across their lifecycle and their effects on biological responses, which may differ in degree and mechanism of toxicity due to each nanoclay's unique properties and organic functionalization. For instance, during their as-received usages in free forms in manufacturing environments, workers could potentially be exposed to elevated levels of the airborne nanoclays.[28,29] In addition, high temperatures and the oxidative environment present during the incineration process associated with their disposal[19] can lead to changes in both chemical composition and surface morphology of nanoclays[20,30] that could potentially change their toxicological effect. Establishing life cycle toxicity assessment profiles are essential to prevent deleterious effects associated with inhalation of such particles by workers in both manufacturing and disposal environments. Specifically, Yuwen et al. observed DNA damage in blood cells for workers exposed to high levels of bentonite particles in factories producing such particles.[29]

We designed a systematic study to help determine the potential for inhalation toxicity of the three organically modified Nanomer nanoclays currently used for food packaging applications. Our study uses human immortalized bronchial epithelial cells (BEAS-2B) and primary small airway epithelial cells (SAECs) as established cell lines for assessing toxicity induced via inhalation because they have previously helped assess toxicity of graphene nanoparticles,[31] asbestos,[32] and carbon nanotubes.[33] The SAEC model expands the impact of our study to a more human-related biological platform as primary cells more closely mimic their tissue of origin and further reduce misidentification, contamination,[34] general genetic instability,[35] and lack of functions and markers often encountered with immortalized cellular systems. Additionally, through the use of two epithelial lung cell lines, we were able to further assess the potential toxicity of nanoclays when they deposit in both the bronchioles and distal airways near the terminal bronchiole and alveolar duct, respectively. Our systematic assessment maps and correlates the physical and chemical properties of nanoclays at two points in their life cycle (i.e., production/manufacturing or the end of their life cycle) with their potential to induce toxicity for a better understanding of how nanoclays' deleterious interactions with the cellular systems can be reduced so safe yet effective materials can be produced and implemented in commercial sectors.

2. EXPERIMENTAL METHODS

2.1. Nanoclay Preparation. Four types of commercially available, raw (as-received) MMT clays were obtained from Sigma-Aldrich. Pursuant to the manufacturer specifications, Nanomer PGV (PGV) is an unmodified, hydrophilic bentonite, Nanomer I.31PS (I.31PS) is surface modified with aminopropyltriethoxysilane at 0.5−5 wt % and octadecylamine at 15−35 wt %, Nanomer I.34TCN (I.34TCN) is surface modified with methyl dihdroxyethyl hydrogenated tallow ammonium at 25−30 wt %, and Nanomer I.44P (I.44P) is surface modified with dimethyl dialkyl amine at 35−45 wt %. All of the modifications were done at the manufacturing site.

2.2. Thermal Degradation. Samples of PGV, I.31PS, I.34TCN, and I.44P were thermally degraded using a TGA701 Thermogravimetric Analyzer from LECO; degradation was used to mimic the disposal generation in municipal solid waste plants.[19] Differences in mass from unheated samples were monitored as a function of temperature and used to calculate % content change. Moisture content of the samples (around 0.5 g each) was determined in the 25−105 °C range, in nitrogen, at a rate of 6 °C/min, while high temperature volatile content was determined in the 105−950 °C range, in nitrogen, at a rate of 43 °C/min. Finally, ash content was determined in the 550−900 °C range, in oxygen, at a rate of 15 °C/min (Table S1). The resulting individual byproduct was collected to serve as the end of life cycle sample assessment, i.e., thermally degraded Nanomer PGV (PGV900), thermally degraded Nanomer I.31PS (I.31PS900), thermally degraded Nanomer I.34TCN (I.34TCN900), and thermally degraded Nanomer I.44P (I.44P900).

2.3. Material Characterization. Molecular composition of the samples and their thermally degraded byproducts in dry powder forms was determined via Fourier transform infrared spectroscopy (FTIR, Digilab FTS 7000) equipped with diamond attenuated total reflection (ATR). For each of the samples, a total of 100 scans in the range of 4000−400 cm^{-1} at a resolution of 4 cm^{-1} was coadded/averaged to form the final spectrum.

Surface morphology and elemental composition of the samples were investigated using a Hitachi S-4700 field emission scanning electron microscope (FE-SEM, Hitachi High-Technologies Corporation) equipped with an energy dispersive X-ray spectroscopy (EDX) unit. For the analyses, dry individual powders were mounted on carbon tape, and their surface morphology was examined at 5.0 kV, while their elemental composition was evaluated at 20.0 kV. For surface morphology, samples were also sputter coated for 10 s in vacuum injected with argon using a gold/palladium target. The argon atoms were ionized and collided with the gold/palladium target, causing the metal ions to deposit on the sample in a thin conductive layer of about 3 nm as calculated using the equation $d = kIVt$, where d is thickness, k is a constant value of 0.17, I is plasma current, V is voltage, and t is the time.

The size distribution of the nanoclays and thermally degraded byproducts was determined by dynamic light scattering (DLS) via the Mastersizer 2000 with a Hydro 2000S accessory (Malvern Instruments). For this, samples of PGV, I31PS, I.3TCN, I.44P, PGV900, I.31PS900, I.34TCN900, or I.44P900 were dispersed either in Dulbecco's modified

DOI: 10.1021/acsami.7b06657
ACS Appl. Mater. Interfaces 2017, 9, 32323−32335

Eagle's medium (DMEM, Life Technologies) containing 5% fetal bovine serum (FBS) or in small airway growth medium (SAGM, Lonza) with SingleQuots Kit (Lonza) containing bovine pituitary extract, hydrocortisone, human epidermal growth factor, epinephrine, transferrin, insulin, retinoic acid, triiodothyronine, gentamicin/amphotericin-B, and 1% bovine serum albumin (BSA). Also, the nanoclays and byproducts were dispersed in a control, phosphate buffered saline (PBS, Lonza), and in distilled water containing 0.15 mg/mL Survanta, a pulmonary surfactant.[36] The solutions were then bath sonicated and dropped into the Hydro 2000S until laser obscuration was within 10−20%. The size analysis was performed 3 consecutive times with a stirrer speed of 1750 rpm and under continuous sonication in the Hydro 2000S accessory.

2.4. Cell Culture. Immortalized human bronchial epithelial cells (BEAS-2B) from American Type Culture Collection (ATCC) were cultured in 100 mm dishes (Corning, In(c) in DMEM containing 5% FBS, 1% L-glutamine, and 1% penicillin−streptomycin (all reagents were purchased from Life Technologies). The cells were incubated at 37 °C, 5% CO_2, and in an 80% relative humidity; consistent subculturing took place using 0.05 or 0.25% trypsin (Invitrogen). Before each experiment, cells were grown to a monolayer of 90−100% confluency, and cells in the 3rd−6th passage were used.

Additionally, small airway epithelial cells (SAECs) were cultured in SAGM with SingleQuots Kit and 1% penicillin−streptomycin (Life Technologies). Cells were seeded into T-25 flasks (Corning, In(c), grown to 75−80% confluency, and subsequently split (5 passages total). All experiments completed with SAECs were performed using the same passage number.

2.5. Half Maximal Inhibitory Concentration (IC_{50}). BEAS-2B cells and SAECs were seeded into 12 well plates (Thermo Scientific) at densities of approximately 1.5×10^5 and 2.0×10^5 cells/mL, respectively. After 24 h, the cells were treated with PGV, I.31PS, I.34TCN, I.44P, or their thermally degraded byproducts at various doses ranging from 0 to 197 $\mu g/cm^2$ (i.e., 0, 0.03, 0.3, 13, 26, 66, 132, and 197 $\mu g/cm^2$). To ensure an effective dose metric and uniform dosage distribution per well, the dose is reported in $\mu g/cm^2$ with the analysis considering the area of the specific well into which the cells were seeded and the initial dilution of nanoclays to form $\mu g/mL$ solutions. Before addition to the respective wells, each nanoclay or byproduct sample was sonicated for 10 min in a bath sonicator (2510 Branson; 100 W) with the concentrations used for exposure being serial dilutions from the original stock; cells in only media served as controls. After 24 h of exposure to individual treatment, the treated cells (as well as the controls) were washed to remove the nanoclays and byproducts, trypsinized, and stained with 0.4% trypan blue solution (Invitrogen). Subsequently, 10 μL of the sample containing the stained cells was added to a hemocytometer, and the number of cells in the 4 outer grids was counted through the use of the Leica DM IL optical microscope (Leica Microsystems) and a 10× objective. Analyses of the cellular proliferation postexposure were used to extrapolate IC_{50} values that would also be used in the remaining cellular assays. At least six replicates were performed for BEAS-2B cells at each dose, and four replicates for SAECs were performed at each dose.

2.6. Cellular Imaging. To evaluate changes in cell morphology, BEAS-2B cells and SAECs were seeded at densities of 1.5×10^5 and 2.5×10^5 cells/mL, respectively, in 24-well plates. After 24 h the cells were treated with the as-received nanoclays and thermally degraded byproducts and dispersed in media via a bath sonicator at their respective determined IC_{50} dose. After 24 h of treatment, the cells were imaged through use of a Leica DM IL optical microscope (Leica Microsystems) with a 10× objective. Two replicates were performed with 10 images per replicate taken at random spots within the well for each control and treatment.

2.7. Extracellular Reactive Oxygen Species. BEAS-2B cells were seeded into 24 well plates at a density of approximately 1.5×10^5 cells/mL. After 24 h, the cells were treated with nanoclays and byproducts dispersed in media through use of a bath sonicator at their respective determined IC_{50} value; cells exposed to only media served as control samples. After 24, 48, and 72 h of treatment, 50 μL of the media was transferred from the 24-well plate to its respective well in a black-bottomed 96-well plate (Corning, In(c). Subsequently, 50 μL of PBS was added to each well in the 96-well plate. Fifty microliters of the extracellular ROS assay reagent, Lumigen ECL Plus (Lumigen, In(c), was also added to each well. The samples were subsequently incubated at room temperature for 5 min in the dark before luminescence was evaluated using a FLUOstar OPTIMA plate reader (BMG LABTECH) at 600 nm. Media and treated media containing nanoclays or byproducts suspended in solution served as blanks. Respective cellular measurements of the samples were evaluated after subtracting the blanks to determine the effect treatment had on extracellular ROS. It has been determined that Lumigen reagent assays generate chemiluminescent responses specific to extracellular ROS.[37] Four replicates were performed for each treatment.

2.8. Statistical Analyses. The cellular experiments were repeated at least four times for each one of the samples (with the exception of cellular imaging). All tables are presented as the average value (±) standard deviation (SD) values. All graphs are presented as the mean value of the number of indicated replicates with (±) standard error (SE) bars. Excel and Origin (OriginLab) were used to determine the IC_{50} value for each of the nanoclays and thermally degraded byproducts through use of a best-fit line (either logistic, exponential, or logarithmic) for each individual replicate with each nanoclay or byproduct treatment containing at least four replicates. Significance was determined by one-way analysis of variance ANOVA with $p < 0.05$* indicating significance.

3. RESULTS AND DISCUSSION

We aimed to provide insights into the toxicity mechanisms associated with human exposure to nanoclays in both manufacturing and disposal areas. For this, we first selected a regiment of four nanoclays, namely one pristine (PGV) and three organically modified nanoclays (I.31PS, I.34TCN, and I.44P) with different physicochemical properties and with relevant implementation in current food packaging applications.[7] Specifically, the modifier for I.31PS consists of a long alkyl tail and a silane coupling agent (Figure 1a).[17] I.34TCN's modifier consists of a long alkyl chain and two hydroxyl molecules,[17] while the modifier for I.44P consists of two long alkyl chains.[17] Secondly, we thermally degraded these nanoclays in conditions aimed to mimic their disposal at the end of their individual life cycles and created resulting byproducts. To assess possible deleterious pulmonary effects, two in vitro cellular models were exposed to as-received nanoclays and their incinerated byproducts. Immortalized human bronchial epithelial cells (BEAS-2B) and small airway epithelial cells (SAECs), previously used for pulmonary toxicity in occupational studies, provided sensitive models for known nanomaterial deposition areas in the lung[38] and served as a validation tool of toxicity of nanoclays. The results are included below.

3.1. Materials Preparation and Characterization. To help evaluate the physicochemical characteristics of the samples being assessed, we compared nanoclays and their byproducts. Specifically, the thermally degraded byproducts of the pristine (PGV) and the three organically modified nanoclays (I.31PS, I.34TCN, and I.44P) were obtained at temperatures up to 950 °C in three different temperature regimes known to mimic incineration conditions at the end of the food packaging product lifecycle[19] (Figure 1b). The moisture, high temperature volatiles, and ash contents of the resulting byproducts were determined in the range of 25−105 and 105−950 °C in nitrogen for moisture and volatile contents, while ash content was assessed in the range of 550−900 °C in oxygen.

Analyses showed that all the modified nanoclays had an amount of moisture significantly lower relative to that of the pristine nanoclay (Table 1), presumably a result of their greater hydrophobicity resulted from individual chemical functionalization with

DOI: 10.1021/acsami.7b06657
ACS Appl. Mater. Interfaces 2017, 9, 32323−32335

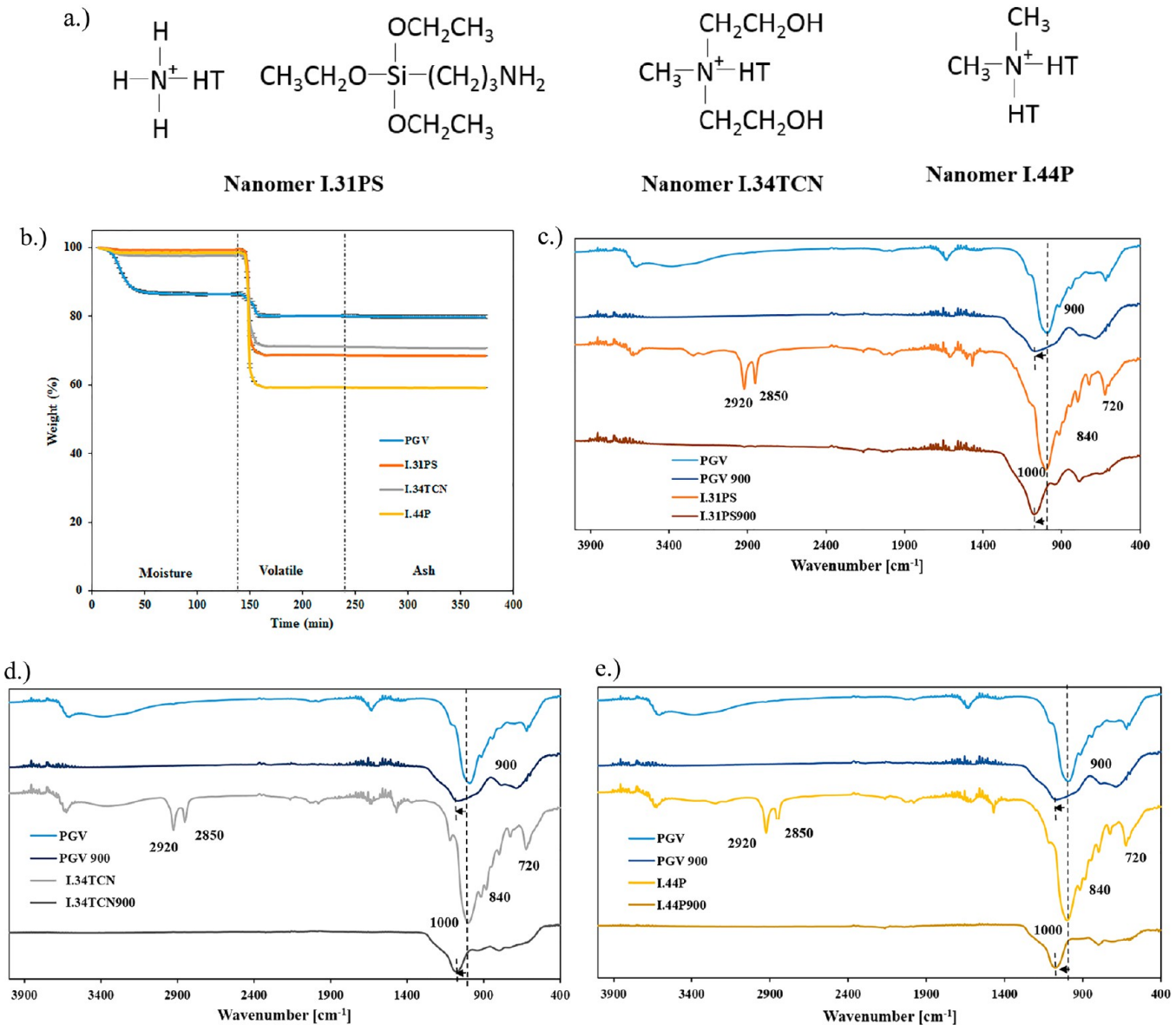

Figure 1. (a) Chemical structures of the organic modifiers present in I.31PS, I.34TCN, and I.44P. (b) Thermal degradation profile of PGV and the 3 organically modified nanoclays (n = 2). FTIR spectrum for (c) I.31PS, (d) I.34TCN, and (e) I.44P along with their thermally degraded byproducts, all relative to PGV and PGV900 (n = 2).

Table 1. Percent of Moisture, High Temperature Volatiles, Ash, and Fixed Carbon Present in the Nanomer Nanoclays Determined by TGA[a]

	moisture	high temperature volatiles	ash	fixed carbon
PGV	13.51 ± 0.71	6.41 ± 0.06	79.78 ± 0.67	0.31 ± 0.10
I.31PS	0.66 ± 0.05*	30.53 ± 0.01*	68.50 ± 0.05*	0.32 ± 0.08
I.34TCN	2.25 ± 0.27*	26.50 ± 0.08*	70.69 ± 0.18*	0.58 ± 0.16
I.44P	1.48 ± 0.13*	39.23 ± 0.12*	59.20 ± 0.06*	0.10 ± 0.06

[a]The symbol * indicates a significant difference between PGV and the organically modified nanoclays (n = 2).

an organic modifier known to replace adsorbed water normally found in pristine nanoclays,[39] therefore minimizing the overall amount of free water to be released.[40,41] The modified nanoclays also showed a significantly higher amount of high temperature volatile content and a significantly lower amount of ash content relative to that of the pristine nanoclay. This is presumably due to the degradation of the organic modifier which has previously been shown to be released within the 200−500 °C temperature range.[40,41] Further, out of the modified nanoclays themselves, I.44P seemed to have the highest amount of high temperature volatile content of around 39% along with the lowest amount of ash content of around 59%, respectively, presumably due to the chemical structure of its organic modifier, which is made up of 2 long alkyl chains which differs from the one of I.31PS and I.34TCN, each only having one long alkyl chain.[17]

DOI: 10.1021/acsami.7b06657
ACS Appl. Mater. Interfaces 2017, 9, 32323−32335

The modified nanoclays also experienced a greater weight loss when compared to that of pristine PGV, all within the temperature range of 400−800 °C (Figure 1b) with I.31PS and I.34TCN experiencing similar amounts of weight loss of about 32 and 30%, respectively, while I.44P experienced a greater weight loss of around 40%. The observed differences are presumably due to the weight percentages (wt %) and chemical composition of the individual organic modifiers used during functionalization as well as their roles in the individual nanoclay's degradation profile,[41] with I.44P's organic modifier being added at 45 wt %, while the organic modifiers of I.31PS and I.34TCN were reported to be added up to 40 and 30 wt %, respectively, via manufacturer specifications. Our analyses are supported by Xie et al. that showed that the amount of organic modifier released in degradation studies is dependent on the interlayer spacing and architecture of the modifier and its integration during nanoclay functionalization.[42] Lastly, PGV seemed to have a more gradual weight loss in the 400−800 °C range when compared to the functionalized nanoclays, which is probably associated with the MMT structure breakdown in which hydroxyl groups incorporated within the crystal lattice are being dehydrated within the temperature range of 500−800 °C.[41]

Physicochemical characterization of the nanoclays and their thermally degraded byproducts was performed via FTIR, scanning electron microscopy (SEM), and elemental composition via energy dispersive X-ray spectroscopy (EDX). Results of the thermally degraded byproducts are reported relative to the representative nondegraded form of the respective nanoclay being investigated. Specifically, FTIR analysis of the characteristic peak of MMT at 1000 cm^{-1}, indicative of Si−O−Si stretching vibration of silicates,[22,40] was observed for all the nanoclays. However, the peak was shifted to a higher wavelength for the thermally degraded byproducts (Figures 1c−e) when compared to their as-received counterparts. Further, all of the as-received nanoclays also displayed a peak at 900 cm^{-1} indicative of Al−OH−Al deformation of aluminates,[22,40,43] while the organically modified as-received nanoclays displayed a peak at 840 cm^{-1}, presumably a result of the deformation of OH linked to Al^{3-} and Mg^{2-}, respectively.[43] Previous analysis showed that peaks at 790 and 630 cm^{-1} are associated with Si−O groups[43] and out of the plane vibration of the Al−O group,[44] respectively.

Additionally, the 3 as-received organically modified nanoclays also had peaks at 2920, 2850, and 720 cm^{-1}, respectively, presumably resulting from the asymmetric and symmetric stretching of their C−H groups included in methylene or alkane rock of CH_2 for alkanes with 7 or more carbons, respectively,[22,40,43] and indicative of the incorporation of their respective organic modifiers. The three peaks were however no longer present in the spectra of the thermally degraded byproducts of these nanoclays, confirming their organic modifiers degradation.[40] Additionally, the peak around 3600 cm^{-1} with small repeated peaks moving out toward 3800 cm^{-1} for the as-received nanoclays, indicative of silanol groups on the SiO_2 tetrahedral sheets,[45] was no longer present for the thermally degraded byproducts. Along with the shift recorded for the 1000 cm^{-1} peak, the only other peaks remaining for the thermally degraded byproducts were at 780 and 640 cm^{-1}, respectively, and are presumably associated with Si−O groups[43] and Si−O−Si bending.[43] Moreover, the peaks associated with Al−OH−Al deformation and OH linked to Al^{3-} and Mg^{2-} were no longer present for any of the byproducts, again showing the degradation of the aluminosilicate lattice due to the loss of structural water.[40−42]

SEM surface morphology analyses revealed layered platelet surfaces (Figures 2a−d) for all the nanoclays being investigated with I.44P appearing to have a sharper, more defined platelet-like geometry when compared to the other nanoclays being investigated. PGV and I.34TCN displayed similar morphologies in that their platelet edges seemed smoother, i.e., more rounded, relative to those of I.31PS and I.44P. Also, while I.31PS had a morphology similar to that of I.44P, it did not seem to contain as many platelets, thus revealing a slightly smoother aspect of its surface.

The observed SEM differences are attributed to the presence of the organic modifiers and their individual integration because previous analyses showed that functionalization of pristine nanoclays could influence their basal spacing.[46] In particular, basal spacing was shown to increase with increasing cation exchange capacity of a modifier[46] or with increasing alkyl length.[42]

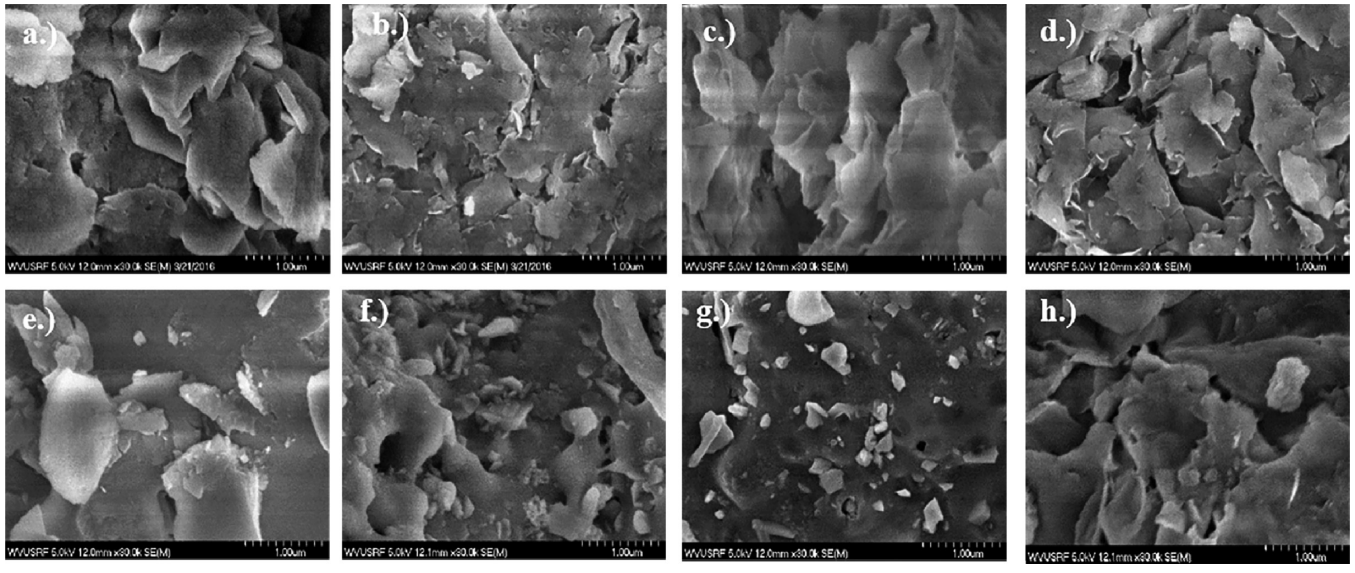

Figure 2. Surface morphology of (a) PGV, (b) I.31PS, (c) I.34TCN, and (d) I.44P and thermally degraded (e) PGV900, (f) I.31PS900, (g) I.34TCN900, and (h) I.44P900 as determined by SEM.

DOI: 10.1021/acsami.7b06657
ACS Appl. Mater. Interfaces 2017, 9, 32323−32335

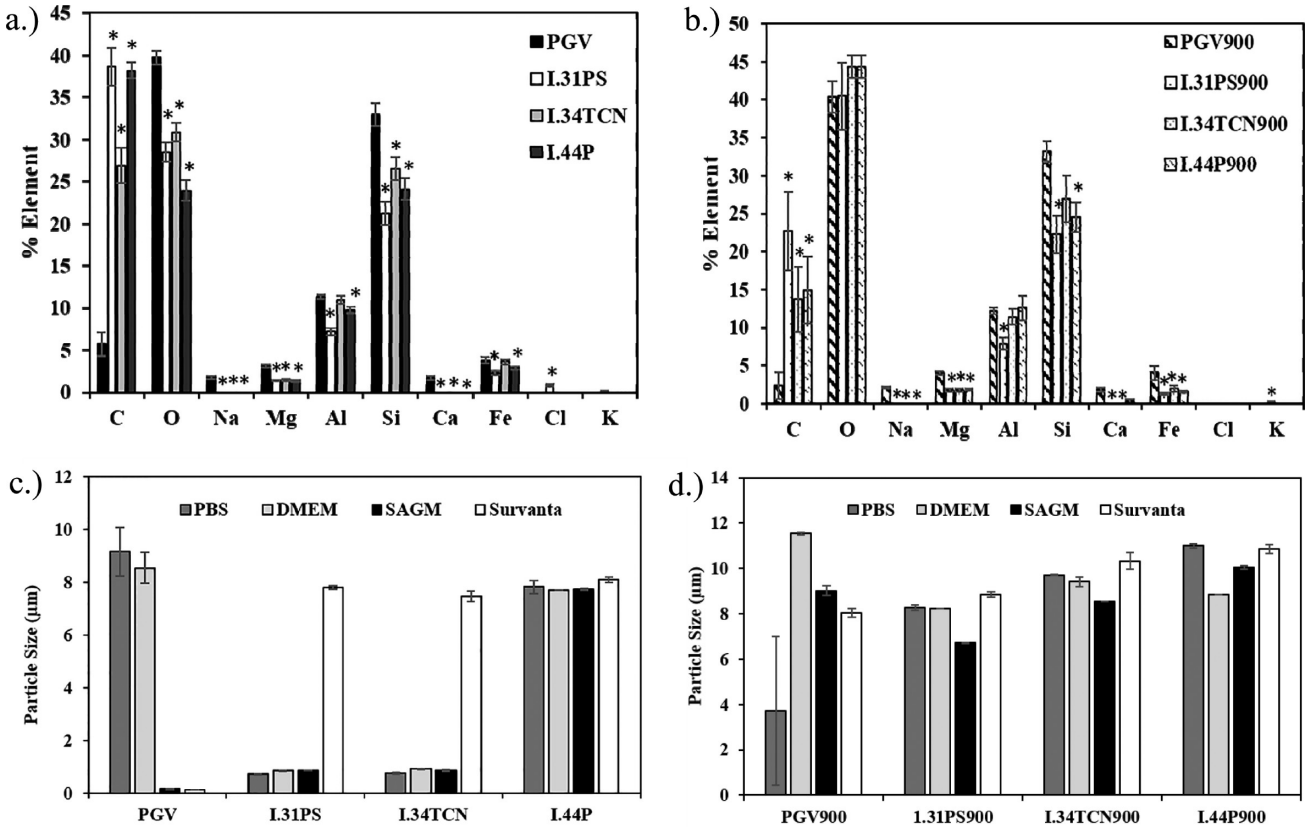

Figure 3. Elemental composition of (a) as-received nanoclay and (b) their thermally degraded byproducts as determined by EDX at 1 μm (n = 10). The symbol * indicates significant differences between the unmodified nanoclay (PGV/PGV900) and the organically modified nanoclays. Average size of <90% of (c) the as-received nanoclays in solutions of PBS, DMEM, SAGM, or Survanta (d) as well as their byproducts (n = 3).

Such increases are presumably due to lowering of the surface energy of the platelets upon introduction of the modifier, thus allowing for their easier separation and better mixing within polymer matrixes during manufacturing of composites.[12] The easier dispersion also was shown to allow for better exfoliation within such polymer matrixes,[4] thus resulting in nanocomposites with enhanced properties such as increased mechanical strength[8] and barrier properties[8] when compared to the neat polymer.[8] Further, previous analysis showed that structure of the nanoclay is influenced by the lateral layer arrangements of the modifiers[46] and is also dependent on the concentration of the modifier used as well as the degree into which the organic molecules are able to fit/adsorb into the nanoclay individual platelet surface.[46]

Thermal degradation caused a loss in the platelet morphology for all the byproducts but I.44P900, which seemed to display platelets with smoother edges relative to those of its nondegraded form (Figures 2e–h). PGV900 also displayed a smoother surface, while both I.31PS900 and I.34TCN900 displayed a fragmented surface with platelets jutting out, potentially due to slower degradation due to the organic modifier. The loss in platelet structure recorded upon thermal degradation was most likely caused by the high temperatures encountered, which could cause their breakdown likely by dehydroxylation of their aluminosilicates' lattice.[42,46] This is supported by previous study by Ounoughene et al., who also observed a change in morphology of halloysite nanotubes (HNTs) after their exposure to high temperatures (beyond 1000 °C).[20]

EDX showed that the as-received organically modified nanoclays had significantly higher amount of carbon relative to their pristine counterparts (Figure 3a). Additionally, they also had significantly lower amounts of oxygen, sodium, magnesium, silicon, and calcium relative to PGV. These changes in elemental composition further confirmed the individual organic modifier functionalization.[39] Moreover, EDX analyses showed that I.34TCN had a lower amount of carbon and higher amount of oxygen relative to those amounts in I.44P and I.31PS, again indicative of the presence of the two hydroxyl moieties associated with the functionalizing modifier.[17] Additionally, I.31PS had a higher amount of oxygen relative to that of I.44P, likely due to the presence of the silane coupling agent which contains carbon and oxygen.[17]

After thermal degradation, all of the nanoclays experienced decreases in their respective carbon contents (up to 40–60% loss) and increases in their oxygen (up to 40–85% increase), magnesium, aluminum, and silicon contents, respectively (Figure 3b). These changes were significant only for the organically modified nanoclays, most likely due to the loss of their individual organic modifiers. Lastly, the organically modified nanoclays had around 40% decrease in their iron contents after thermal degradation. The general trends in elemental composition between PGV and the modified nanoclays also persisted after thermal degradation relative to the as-received forms (Table S2). Further, the only significant difference between PGV and PGV900 was an increase in magnesium, showing that the organic modifiers played a large role in the changes observed in elemental composition due to thermal degradation.

3.2. Dispersity Analysis of Nanoclays and Byproducts.

Considering that particle size and distribution have been

DOI: 10.1021/acsami.7b06657
ACS Appl. Mater. Interfaces 2017, 9, 32323–32335

demonstrated to influence the toxicity of materials[47] as well as internalization into exposed cells,[47] we first assessed nanoclays and byproducts dispersion in cellular media. Such analyses were also expected to provide insights into any sedimentation and/or possible diffusion of the materials, thus helping to ensure that there are no-mass transfer limitations when exposure to cells is attempted, thus limiting an uneven exposure and localized toxicological effects.

Size distributions of the nanoclays and byproducts were assessed by dynamic light scattering (DLS); for this, samples were dispersed in their cell-specific media. A pulmonary surfactant (Survanta) of 90% lipid and 10% protein was also used to provide a model of similar consistency to the pulmonary surfactant environment of humans.[48] How a particle interacts with a pulmonary surfactant will affect its deposition on and interaction with lung cells, its clearance, and overall alveolar surface tension.[49] Analyses are reported relative to control buffer solution (phosphate buffered saline: PBS) normally used for cellular studies.

Overall, the organically modified nanoclays (with the exception of I.44P) had smaller sizes in PBS and Dulbecco's modified Eagle's medium (DMEM), whereas larger sizes were observed when the modified nanoclays were placed in small airway growth medium (SAGM) and Survanta, respectively, all relative to the pristine nanoclay (PGV; Table S3). Specifically, analyses showed that 90% of the I.44P dispersed in either PBS, DMEM, SAGM, or Survanta all had similar sizes and were smaller than 8 μm (Figure 3c). Moreover, 90% of the I.31PS and I.34TCN nanoclays dispersed in either control PBS, DMEM, or SAGM were smaller than 0.9 μm. Both I.31PS and I.34TCN displayed an increase in size when in Survanta with 90% of these nanoclays being under 8 μm. Lastly, 90% of the PGV dispersed in either SAGM or Survanta were smaller than 0.15 μm. Particle size increased when the nanoclay was placed in PBS and DMEM, with 90% of it ranging under 9 μm for both solutions, respectively. The specific distribution ranges are summarized in Tables S4–7.

The observed differences are likely due to the complex interactions of nanoclays with proteins and lipids in the media they were dispersed in,[50,51] formations of protein corneas,[50] and/or particle repulsion.[52] Specifically, particles that contain long hydrophobic chains such as I.44P have been previously shown to have increased protein-binding sites[53] relative to their more hydrophilic counterparts, likely leading to an increased agglomeration via interparticle−protein bridges.[54] Additionally, the hydrophobic portions of the proteins may associate with the more hydrophobic nanoclays such as the I.44P to further cause agglomeration.[51]

In the case of PGV, the hydrophilic portions of the proteins may also bind strongly to the nanoclay's hydrophilic surface,[51] also causing particle agglomeration as seen in DMEM.[50] However, PGV had a large decrease in size when placed in SAGM (relative to DMEM), signifying the influence of media composition.[55] Specifically, because SAGM has a greater variety of proteins and growth factors present relative to the DMEM, it could possibly allow for a more varied protein adsorption profile to this nanoclay and thus an increase in its dispersity. Similarly, I.34TCN and I.31PS likely had less agglomeration in both DMEM and SAGM due to their relative intermediate hydrophobicity compared to that of PGV, resulting from their organic modifiers functionalization, which could presumably cause heterogeneous[51] or less protein adsorption[55] and thus a better dispersion.[55] Additionally, their organic modifiers containing hydroxyl (I.34TCN) and amine (I.31PS) groups could be more prone to interaction with proteins via hydrogen bonding, van der Waals forces, and electrostatic interactions, causing clay repulsion[52] to be recorded as an increase in their individual dispersity.

Overall, solution type did not appear to largely influence the size distributions of the dispersed byproducts; however, it did cause an increase in the individual particle size distributions (Figure 3d). For instance, 90% of the I.44P900 dispersed in DMEM, SAGM, Survanta, and PBS was smaller than 9, 10, 11, and 11 μm, respectively. I.31PS900 displayed similar size distributions in all 4 solutions, with 90% of its particles smaller than 9 μm in PBS, DMEM, and Survanta and 90% of its particles smaller than 7 μm in SAGM only. Ninety percent of the I.34TCN900 dispersed in DMEM, SAGM, and Survanta was smaller than 10, 9, and 11 μm, respectively; 90% of the particles in PBS was smaller than 10 μm. Finally, 90% of the PGV900 dispersed in DMEM, SAGM, or Survanta was smaller than 12, 9, and 8 μm, respectively. Additionally, there were no longer any differences between the organically modified nanoclays (i.e., difference in size for I.31PS and I.34TCN relative to I.44P in DMEM, SAGM, and PBS) after thermal degradation, further confirming that once the organic modifier was removed and the platelet structure was melted and fused, no platelet exfoliation or breakup of loose agglomerates might have taken place; thus, the surface chemistry and resulting molecular interactions might have changed. In particular, because the byproducts no longer have their organic modifiers present, this would likely decrease the amount of adsorbed protein and, dependent on the modifier, the variety of proteins being adsorbed, thus in turn decreasing the stability of the suspensions[56] and resulting in the recorded larger sizes.

Lastly, the different size distributions observed for nanoclays or byproducts in Survanta could be a result of Survanta's high content of phospholipids,[49] which could largely change the agglomeration states of the dispersed materials. Specially, the increased hydrophobicity of the modified nanoclays relative to that of PGV likely caused an increased agglomeration and higher interactions with the hydrophobic tails of the phospholipids.[48] Sauer et al. found similar results for hydrophobic nanoparticles that generally seemed to agglomerate more when in the presence of lipids and proteins relative to their more hydrophilic counterparts.[57]

3.3. Toxicity Screening Based on Nanoclays' Physicochemical Properties. Upon dispersity analysis, nanoclays and byproducts dispersed in the complementary media were used in different concentrations (i.e., 0−197 μg/cm^2) and exposed to BEAS-2B cells and SAECs for 24 h. The dose range was chosen to mimic exposure in manufacturing and disposal condition areas with light exposure being defined as the minimal concentration that could lead to inhalation in a manufacturing or disposal environment, and acute exposure being defined as a 45-year working lifetime exposure based on 8 h/day and 50 weeks/year taking into account particle and lung characteristics.[58] The resulting IC_{50} values (concentration of the nanoclays or byproducts that inhibit cell growth by 50%) were extrapolated from the dose response trend lines derived from raw data (Table S8). IC_{50} is an acceptable mean for early measure and comparison of particle cytotoxicity[59] and could help identify early deleterious mechanisms associated with nanoclay exposure to cellular systems.

Overall, the as-received nanoclays, with the exception of I.44P in SAECs, displayed a greater cytotoxicity relative to their thermally degraded byproducts when exposed to both BEAS-2B cells and SAECs (Figure 4a). In addition, organically modified nanoclays showed toxicity higher than that of their pristine

DOI: 10.1021/acsami.7b06657
ACS Appl. Mater. Interfaces 2017, 9, 32323−32335

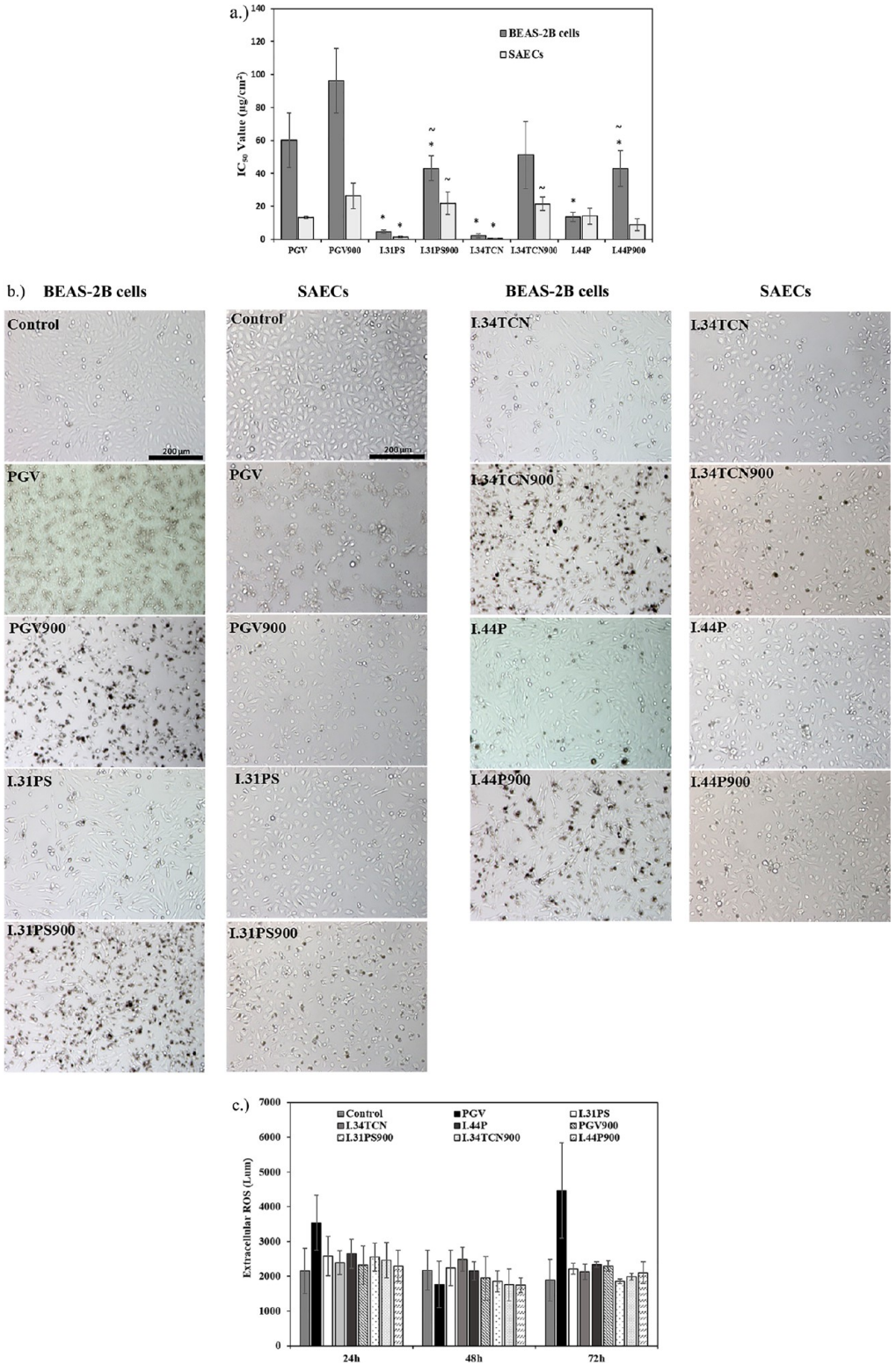

Figure 4. (a) IC_{50} values ($\mu g/cm^2$) for BEAS-2B cells and SAECs treated with as-received nanoclays and byproducts. The symbols * and ~ indicate significant differences between the unmodified nanoclay (PGV/PGV900) and the organically modified nanoclays and between the as-received nanoclay and its thermally degraded byproduct, respectively ($n \geq 4$ for each treatment). (b) Representative optical images of BEAS-2B cells and SAECs treated with as-received nanoclays and byproducts at their respective IC_{50} dose after 24 h of exposure. (c) Extracellular ROS production by BEAS-2B cells after treatment with as-received nanoclays and byproducts at their respective IC_{50} dose over 72 h ($n = 4$).

counterpart (PGV), again with the exception of I.44P in SAECs. The byproducts showed similar toxicity with the PGV900 for the BEAS-2B cells (with PGV900 being the least toxic), while all the byproducts had a similar toxicity to each other for the SAECs. The highest degree of toxicity was observed for I.34TCN (which has a long alkyl chain and 2 hydroxyl molecules),[17] followed by lower degrees of toxicity for I.31PS (which has a long alkyl tail and a silane coupling agent) and finally I.44P (which has 2 long

DOI: 10.1021/acsami.7b06657
ACS Appl. Mater. Interfaces 2017, 9, 32323−32335

alkyl chains) in both cell lines being investigated. Lastly, SAECs showed a greater sensitivity relative to that of BEAS-2B cells for all the nanoclays and byproducts, with the exception of I.44P.

We hypothesize that the cytotoxicity differences are based on the different interactions of the organic modifier-functionalized nanoclays that could influence particle's degree of hydrophobicity. Previous studies showed that such chains could interact with the cell membrane lipids to cause changes in membrane integrity.[60] For instance, Farcal et al. showed that TiO_2 nanomaterials with a hydrophobic coating were more toxic than their hydrophilic counterpart in murine alveolar macrophages.[60] Additionally, the increased toxicity of I.34TCN relative to that of I.31PS and I.44P was likely due to the presence of bioreactive groups such as hydroxyl present in its organic modifier. Previous studies on particles containing bioreactive groups showed similar results,[61,62] with analysis revealing that such particles could interact with biological macromolecules[61] such as phospholipids and proteins[62,63] via hydrogen bonding and electrostatic interactions,[63] disrupt the cell membranes,[62,63] and initiate apoptosis.[63] Specifically, Zhang et al. showed a decrease in BEAS-2B cell viability upon their exposure to amorphous silica nanoparticles with increased hydroxyl contents.[62] Das et al. found that graphene sheets containing reactive hydroxyl functional groups were more toxic than sheets without these groups and of the same sizes,[61] while Zhang et al. showed that hydroxyl groups can generate ROS[62] to be responsible for damage to macromolecules such as nucleic acids, proteins, and lipids, and for deregulation of cellular signaling pathways associated with cell proliferation, survival, and mitochondrial oxidative stress.[64]

While I.31PS did not contain hydroxyl groups, it did contain a silane coupling agent[17] and an amine group which were shown to also be capable of binding to both organic and inorganic compounds,[65] to allow for interactions with biological molecules containing hydroxyl groups[66] as well as the negatively charged cell membrane.[67] Positively charged particles such as the silane terminated amine groups in I.31PS will also have a better cell internalization[68] which could further contribute to its observed increased toxicity.[63] While the interchange of bioreactive groups with long alkyl chains showed a decrease in toxicity, as observed by the reduction in toxicity of I.44P relative to that of the other two organically modified nanoclays and by previous studies,[68] their presence on particles still caused toxicity most likely because of disturbances of hydrophobic interactions between the lipids and proteins and possibly induced changes in cell signaling.[69]

The byproducts were less toxic relative to their as-received counterparts in both cell lines (except for I.44P/I.44P900 in SAECs). This is presumably due to the recorded loss of their organic modifiers,[25,23,22] reduction of their iron contents, and changes in their platelet morphology,[21] as demonstrated by the SEM and EDX analyses, or to the loss of the silanol groups on the SiO_2 tetrahedral sheets of the nanoclays,[45] as demonstrated by the FTIR analysis. Specifically, our EDX analysis confirmed that iron decreased by around 40% in the byproducts, thus causing lower toxicity as supported by previous analysis that showed that high levels of iron promote cell death[70] and decrease ATP production.[71] Additionally, silanol groups (especially the disorganized silanols) have been previously hypothesized to contribute to SiO_2 toxicity.[72]

Along with the presence of the organic modifiers, the size and general solubility of the nanoclays and byproducts may also be contributing to the observed differences in cytotoxicity. As seen by the DLS measurements, smaller sized nanoclays (I.34TCN and I.31PS) seemed to show an increase in cytotoxicity relative to that of the larger as-received nanoclays (PGV and I.44P) as well as their byproducts, presumably due to a resultant higher surface area[73] or higher degree of uptake.[74,75] Results are consistent with previous analysis;[74] specifically, Napierska et al. found that smaller sized particles (14−16 nm diameter) were more toxic relative to their larger sized counterparts (19−335 nm) and were internalized by human endothelial cells at a faster rate.[74] Additionally, Lin et al. found that smaller Stöber silica nanoparticles had hemolytic activity higher than that of larger counterparts, most likely resulting from a larger surface area of such particles.[75] However, PGV displayed the smallest size distribution in SAGM (media for SAECs) yet still had a lower degree of toxicity relative to that of I.34TCN and I.31PS, showing that the chemical composition of the organic modifiers plays a large role in the toxicity profiles of these nanoclays, as detailed above. The resultant smaller size of PGV could have attributed to it having a higher degree of toxicity relative to I.44P though in SAECs, which was not observed in the BEAS-2B cells when I.44P and PGV had a similar size distribution.

Overall, SAECs showed a greater sensitivity (of about 4 to 5 times) for all the nanoclays (except I.44P), while the sensitivity of the primary cells exposed to byproducts was only about 2 to 4 times higher relative to that of BEAS-2B cells. This is presumably due to the fact that primary cells more closely mimic their tissue of human origin; on the contrary, their immortalized counterparts can undergo mutations as well as contain viral genes to influence their overall stability, thus reducing their susceptibility to external agents used for toxicity analysis.[34] Further, immortalized cell lines generally are not as genetically stable as primary cells and lack function and markers often seen in vivo.[35] Our results confirm previous experiments in which primary cells displayed a higher degree of toxicity when compared to immortalized cell lines upon exposure to nanoparticles with similar aspect ratios.[38] Moreover, the general trends in our experiments remained the same between the two cell lines, showing validation of the obtained results and overall confirming that such cell-based systems are suitable models for assessing inhalation toxicity in vitro.

Changes in IC_{50} were complemented by the changes in cell morphology (Figure 4b) which is known to be an indicator of overall cell health.[76,77] Specifically, treatment with the nanoclays and byproducts caused changes in the cellular shape of both cell types relative to the control, more so for the BEAS-2B cells. These cells were more stretched, thin-like structures relative to the more oval shapes displayed by the controls (especially in regards to their exposure to the byproducts). When comparing BEAS-2B cells with the primary cells, it was observed that the immortalized cells had a more stretched profile. Generally, treatment with PGV produced more circular cells than any of the other treatments in both cell lines and also a lower cell confluence especially in primary cells, likely serving as a signal of cell death and thus complementing our IC_{50} values as well as possibly indicating a different mechanistic-based cytotoxic effect.[77] A difference in cytotoxic mechanism is also supported by different slopes of the dose response curves for PGV compared to organically modified nanoclays. For SAECs, exposure seemed to also cause changes in the cell membrane, which could then influence cell−cell and cell−substrate interactions.[76] Additionally, there were changes in the cell monolayer with all of the treatments causing a loss of monolayer integrity relative to controls for both cell lines being investigated over a 72 h time period (Figures S1 and S2). Such changes can further provide insights into the integrity of the

DOI: 10.1021/acsami.7b06657
ACS Appl. Mater. Interfaces 2017, 9, 32323−32335

tight junctions of the epithelial cells and mechanisms of toxicity because it is known that in the lung, the epithelial cells serve as a barrier to prevent the entrance of inhaled particles and pathogens.[78]

Our results overall hint that treatment with nanoclays or byproducts may cause cytoskeleton alterations[76] which may eventually lead to changes in cell mechanics,[79] differentiation, and organization.[80] Similarly, Snyder et al. showed changes in cellular morphology of primary human bronchial epithelial cells from a cuboidal shape to a spindle-shaped, fibroblastoid appearance upon treatment with multiwalled carbon nanotubes.[78] Further, our systematic analysis showed that the observed differences in cytotoxicity are most likely due to synergistic effects resulting from (1) the presence of the organic modifiers and their surface chemistry and/or (2) the individual nanoclay or byproduct particle size and surface area and general dispersibility. Synergism has been previously reported for other materials where the combined effects of size, shape, solubility, and/or surface functionalization all contributed to the toxicity profile of the material.[81,82] For instance, Tarantola et al. found that cetyltrimethylammonium bromide (CTAB)-coated spherical particles were more toxic than rod-shaped ones, due not only due to the shape but also due to the way such shape influenced cluster formation and release of the CTAB.[81] Xia et al. found that the composition of metal oxide nanoparticles influenced toxicity; however, the degree of toxicity of the metal oxide was also dependent on its solubility in the media.[82] On the basis of our results, it is likely that the chemical composition of the organic modifier is influencing the degree of toxicity, both directly and indirectly due to such modifier composition and effect on the size and dispersibility of the nanoclays. Such toxic effects were diminished when the cells were exposed to the byproducts.

The observed synergism also implies that setting up rather simplistic platforms for toxicity evaluation will not provide a realistic or viable assessment strategy. Extracellular quantitative luminescence ROS assays[62] were previously shown to be reliable and help provide information on oxidative stress and cellular metabolism[64] or damage to macromolecules.[64] Indeed, our control analysis showed that when using the extracellular ROS assay, our results were inconclusive (Figure 4c). In particular, there was no significant trend observed in the cell response with treatment, and moreover, there was a large variability in the extracellular ROS production. A similar response was also observed for doses above and below the IC_{50} value for each nanoclay and byproduct (Figure S3). This could be due to the interaction of the nanoclays with the reagent. Our study accentuates the controversy of using such reagent for toxicity screening and adds to the bases of other studies that showed[22] or did not show[83] ROS generation for cells exposed to nanoclays. In particular, Maisanaba et al. did not observe any ROS generation for Cloisite Na^+ and Cloisite 30B in HepG2 cells up to a dose of 88 μg/mL;[83] however, Lordan et al. found that Cloisite Na^+ did cause ROS generation in HepG2 cells at doses 50 μg/mL higher.[22]

Our study is the first to show that if one is to implement a platform for toxicity screening of nanoclays during their life cycle, the overall functionality of the material needs to be tested with functionality encompassing not only physicochemical characteristics of the as-produced material, but also its changes in a variety of conditions that reflect product implementation and disposal. Further, our study shows that cellular system complexity needs to be accounted for, as differences in toxicity may be observed between cell lines and could be due to the different cell line sensitivity as well as any related cellular changes upon cell line transformation. Only through such a dynamic interplay that could affect both the product personality as well as its shelf life and interactions could one fully evaluate product safety characteristics and impose viable disposal measures.

4. CONCLUSIONS

Our study showed that the chemical composition of individual organic modifiers used for nanoclay functionalization played a large role in their interactions with cellular systems. Specifically, differences in organic modifiers caused differential size distributions in dispersion cellular media and differential degrees of toxicity upon their or thermally degraded byproducts exposure to lung epithelial cells. The organically modified nanoclays I.34TCN and I.31PS displayed the highest degree of toxicity, followed by I.44P, all relative to that of the pristine PGV. On the basis of the chemical structure of their modifiers, it can be determined that modifiers containing bioreactive groups such as hydroxyl are more toxic relative to the modifiers containing long alkyl chains, likely due to increased interaction with biological macromolecules. Further, the composition of the bioreactive group was shown to influence toxicity, as the modifier containing hydroxyl (I.34TCN) was more toxic relative to the one containing amine and silane (I.31PS). Finally, the byproducts displayed a loss in toxicity, likely due to the loss of their organic modifier, changes in size, shape, and elemental composition. Such changes in toxicity profiles of the as-received nanoclays relative to their byproducts emphasize the importance of examining such materials at all stages in their life cycle where human exposure might occur. Understanding how the physical and chemical properties of such materials influence toxicity can aid in safer design functionalities while still maintaining beneficial properties to make them miscible with polymer matrixes for food packaging applications.

■ ASSOCIATED CONTENT

Supporting Information

The Supporting Information is available free of charge on the ACS Publications website at DOI: 10.1021/acsami.7b06657.

Additional material characterization and dispersity analyses of the nanoclays and byproducts and additional cell images and ROS data from 24 to 72 h (PDF)

■ AUTHOR INFORMATION

Corresponding Author

*E-mail: cerasela-zoica.dinu@mail.wvu.edu; Tel.: +1 304 293 9338; Fax: +1 304 293 4139.

ORCID

Cerasela Zoica Dinu: 0000-0002-6474-6771

Notes

The authors declare no competing financial interest.

■ ACKNOWLEDGMENTS

This work was supported by National Science Foundation (NSF) Grants 1434503 and 1454230 and the National Institutes of Health (NIH; Grant R01-ES022968). The authors acknowledge use of WVU Shared Research Facilities and the WVU Analytical Lab. The findings and conclusions in this report are those of the authors and do not necessarily represent the views of the National Institute for Occupational Safety and Health. Use of brand name does not constitute product support.

DOI: 10.1021/acsami.7b06657
ACS Appl. Mater. Interfaces 2017, 9, 32323−32335

REFERENCES

(1) Camargo, P. H. C.; Satyanarayana, K. G.; Wypych, F. Nanocomposites: Synthesis, Structure, Properties and New Application Opportunities. *Mater. Res.* **2009**, *12*, 1−39.

(2) Mitrano, D. M.; Motellier, S.; Clavaguera, S.; Nowack, B. Review of Nanomaterial Aging and Transformations through the Life Cycle of Nano-enhanced Products. *Environ. Int.* **2015**, *77*, 132−147.

(3) Pereira de Abreu, D. A.; Paseiro Losada, P.; Angulo, I.; Cruz, J. M. Development of New Polyolefin Films with Nanoclays for Application in Food Packaging. *Eur. Polym. J.* **2007**, *43*, 2229−2243.

(4) Ray, S.; Okamoto, M. Polymer/layered Silicate Nanocomposites: A Review from Preparation to Processing. *Prog. Polym. Sci.* **2003**, *28*, 1539−1641.

(5) Sahoo, R.; Sahoo, S.; Nayak, P. L. Synthesis and Characterization of Gelatin-Chitosan Nanocomposite to Explore the Possible Use as Drug Delivery Vehicle. *Eur. Sci. J.* **2013**, *9*, 135−141.

(6) Mallakpour, S.; Dinari, M. Synthesis and Properties of Biodegradable Poly (vinyl alcohol)/ Organo-nanoclay Bionanocomposites. *J. Polym. Environ.* **2012**, *20*, 732−740.

(7) Silvestre, C.; Duraccio, D.; Cimmino, S. Food Packaging Based on Polymer Nanomaterials. *Prog. Polym. Sci.* **2011**, *36*, 1766−1782.

(8) Paul, D. R.; Robeson, L. M. Polymer Nanotechnology: Nanocomposites. *Polymer* **2008**, *49*, 3187−3204.

(9) Molinaro, S.; Romero, M. C.; Boaro, M.; Sensidoni, A.; Lagazio, C.; Morris, M.; Kerry, J. Effect of Nanoclay-type and PLA Optical Purity on the Characteristics of PLA-based Nanocomposite Films. *J. Food Eng.* **2013**, *117*, 113−123.

(10) Zheng, X.; Wilkie, C. A. Flame Retardancy of Polystyrene Nanocomposites based on an Oligomeric Organically-modified Clay containing Phosphate. *Polym. Degrad. Stab.* **2003**, *81*, 539−550.

(11) Manikantan, M. R.; Sharma, R.; Kasturi, R.; Varadharaju, N. Storage Stability of Banana Chips in Polypropylene Based Nanocomposite Packaging Films. *J. Food Sci. Technol.* **2014**, *51* (11), 2990−3001.

(12) Majeed, K.; Jawaid, M.; Hassan, A.; Abu Baker, A.; Abdul Khalil, H. P. S.; Salema, A. A.; Inuwa, I. Potential Materials for Food Packaging from Nanoclay/natural Fibres filled Hybrid Composites. *Mater. Eng.* **2013**, *46*, 391−410.

(13) Harkki, O. *Biaxially Oriented PLA-Montmorrilonite-Nanocomposite for Barrier Film Applications*; VTT Technical Research Centre of Finland: 2012 (online).

(14) Floody, M. C.; Theng, B. K. G.; Mora, M. L. Natural Nanoclays: Applications and Future Trends-A Chilean Perspective. *Clay Miner.* **2009**, *44*, 161−176.

(15) Campos-Requena, V. H.; Rivas, B. L.; Pérez, M. A.; Garrido-Miranda, K. A.; Pereira, E. D. Polymer/Clay Nanocomposite Films as Active Packaging Material: Modeling of Antimicrobial Release. *Eur. Polym. J.* **2015**, *71*, 461−475.

(16) Tang, Y.; Lewin, M. Maleated Polypropylene OMMT Nanocomposite: Annealing, Structural Changes, Exfoliated and Migration. *Polym. Degrad. Stab.* **2007**, *92*, 53−60.

(17) Feng, J.; Hao, J.; Du, J.; Yang, R. Effects of Organoclay Modifiers on the Flammability, Thermal and Mechanical Properties of Polycarbonate Nanocomposites filled with Phosphate and Organoclays. *Polym. Degrad. Stab.* **2012**, *97*, 108−117.

(18) Yourdkhani, M.; Mousavand, T.; Chapleau, N.; Hubert, P. Thermal, Oxygen Barrier and Mechanical Properties of Polylactide-organoclay Nanocomposites. *Compos. Sci. Technol.* **2013**, *82*, 47−53.

(19) Roes, L.; Patel, M. K.; Worrell, E.; Ludwig, C. Preliminary Evaluation of Risks Related to Waste Incineration of Polymer Nanocomposites. *Sci. Total Environ.* **2012**, *417−418*, 76−86.

(20) Ounoughene, G.; Bihan, O. L.; Chivas-Joly, C.; Motzkus, C.; Longuet, C.; Debray, B.; Joubert, A.; Coq, L. L.; Lopez-Cuesta, J. M. Behavior and Fate of Halloysite Nanotubes (HNTs) When Incinverating PA6/HNTs Nanocomposite. *Environ. Sci. Technol.* **2015**, *49*, 5450−5457.

(21) Verma, N. K.; Moore, E.; Blau, W.; Volkov, Y.; Babu, P. R. Cytotoxicity Evaluation of Nanoclays in Human Epithelial Cell Line A549 using High Content Screening and Real-time impedance Analysis. *J. Nanopart. Res.* **2012**, *14*, 1−11.

(22) Lordan, S.; Kennedy, J. E.; Higginbotham, C. L. Cytotoxic Effects Induced by Unmodified and Organically Modified Nanoclays in Human Hepatic HepG2 Cell Line. *J. Appl. Toxicol.* **2011**, *31*, 27−35.

(23) Sharma, A. K.; Schmidt, B.; Frandsen, H.; Jacobsen, N. R.; Larsen, E. H.; Binderup, M. Genotoxicity of Unmodified and Organo-modified Montmorillonite. *Mutat. Res., Genet. Toxicol. Environ. Mutagen.* **2010**, *700*, 18−25.

(24) Maisanaba, S.; Hercog, K.; Ortuño, N.; Jos, A.; Zegura, B. Induction of Micronuclei and Alteration of Gene Expression by an Organomodified Clay in HepG2 Cells. *Chemosphere* **2016**, *154*, 240−248.

(25) Janer, G.; Fernández-Rosas, E.; Mas del Molino, E.; González-Gálvez, D.; Vilar, G.; López-Iglesias, C.; Ermini, V.; Vázquez-Campos, S. In vitro Toxicity of Functionalised Nanoclays is Mainly Driven by the Presence of Organic Modifier. *Nanotoxicology* **2014**, *8*, 279−294.

(26) Maisanaba, S.; Puerto, M.; Gutièrrez-Praena, D.; Llana-Ruíz-Cabello, M.; Pichardo, S.; Mate, A.; Jordá-Beneyto, M.; Cameán, A. M.; Aucejo, S.; Jos, A. In vivo Evaluation of Activities and Expression of Antioxidant Enzymes in Wistar Rats Exposed for 90 Days to a Modified Clay. *J. Toxicol. Environ. Health, Part A* **2014**, *77*, 456−466.

(27) Stueckle, T. A.; Davidson, D.; Derk, R.; Komberg, T.; Battelli, L.; Friend, S.; Wagner, A.; Gupta, R.; Dinu, C. Z.; Porter, D.; Rojanasakul, L. Life Cycle Assessment of Pre- and Post-incinerated Organomodified Nanoclay for Pulmonary Inflammation and Fibrotic Potential. *Toxicologist* **2017**, *156*, 75−75.

(28) Tsai, C. S. J.; White, D.; Rodriguez, H.; Munoz, C. E.; Huang, C.-Y.; Tsai, C.-J.; Barry, C.; Ellenbecker, M. J. Exposure Assessment and Engineering Control Strategies for Airborne Nanoparticles: an Application to Emissions from Nanocomposite Compounding Processes. *J. Nanopart. Res.* **2012**, *14* (7), 1−14.

(29) Yuwen, H.; Meibian, Z.; Hua, Z.; Xiaxue, L.; Mingluan, X.; Xinglin, F.; Jiliang, H. Genetic Damage and Lipid Peroxidation in Workers Occupationally Exposed to Organic Bentonite Particles. *Mutat. Res., Genet. Toxicol. Environ. Mutagen.* **2013**, *751*, 40−44.

(30) Wagner, A.; Eldawud, R.; White, A.; Agarwal, S.; Stueckle, T. A.; Sierros, K. A.; Rojanasakul, Y.; Gupta, R. K.; Dinu, C. Z. Toxicity Evaluations of Nanoclays and Thermally Degraded Byproducts through Spectroscopical and Microscopical Approaches. *Biochim. Biophys. Acta, Gen. Subj.* **2017**, *1861*, 3406−3415.

(31) Mittal, S.; Kumar, V.; Dhiman, N.; Chauhan, L. K.; Pasricha, R.; Pandey, A. K. Physico-chemical Properties Based Differential Toxicity of Graphene Oxide/reduced Graphene Oxide in Human Lung Cells Mediated through Oxidative Stress. *Sci. Rep.* **2016**, *6*, 1−15.

(32) Wang, X.; Wu, Y.; Stonehuerner, J. G.; Dailey, L. A.; Richards, J. D.; Jaspers, I.; Piantadosi, C. A.; Ghio, A. J. Oxidant Generation Promotes Iron Sequestration in BEAS-2B Cells Exposed to Asbestos. *Am. J. Respir. Cell Mol. Biol.* **2006**, *34* (3), 286−292.

(33) Eldawud, R.; Wagner, A.; Dong, C.; Rojansakul, Y.; Dinu, C. Z. Electronic Platform for Real-time Multi-parametric Analysis of Cellular Behavior Post-exposure to Single-walled Carbon Nanotubes. *Biosens. Bioelectron.* **2015**, *71*, 269−277.

(34) Masters, J. R. W. Human Cancer Cell Lines:Fact and Fantasy. *Nat. Rev. Mol. Cell Biol.* **2000**, *1*, 233−236.

(35) Alge, C.; Hauck, S.; Priglinger, S.; Kampik, A.; Ueffing, M. Differential Protein Profiling of Primary versus Immortalized Human RPE Cells Identifies Expression Patterns Associated with Cytoskeletal Remodeling and Cell Survival. *J. Proteome Res.* **2006**, *5*, 862−878.

(36) Jobe, A. H. Pulmonary Surfactant Therapy. *N. Engl. J. Med.* **1993**, *328*, 861−868.

(37) Uy, B.; McGlashan, S. R.; Shaikh, S. B. Measurments of Reactive Oxygen Species in the Culture Media Using Acridan Lumigen PS-3 Assay. *J. Biomol. Techniq.* **2011**, *22*, 95−107.

(38) Rujanapun, N.; Auevirivavit, S.; Boonrungsiman, S.; Rosena, A.; Phummiratch, D.; Riolueang, S.; Chalaow, N.; Viprakasit, V.; Maniratanachote, R. Human Primary Erythroid Cells as a More Sensitive Alternative in vitro Hematological Model for Nanotoxicity

DOI: 10.1021/acsami.7b06657
ACS Appl. Mater. Interfaces 2017, 9, 32323−32335

Studies: Toxicological Effects of Silver Nanoparticles. *Toxicol. In Vitro* **2015**, *29* (8), 1982−92.
(39) Ribeiro, S. P. S.; Estevao, L. R. M.; Nascimento, R. S. V. Effect of Clays on the Fire-retardant Properties of a Polyethlenic Copolymer Containing Intumescent Formulation. *Sci. Technol. Adv. Mater.* **2008**, *9*, 1−7.
(40) Cervantes-UC, J. M.; Cauich-Rodriguez, J. V.; Vazquez-Torres, H.; Garfias-Mesias, L. F.; Paul, D. R. Thermal Degradation of Commercially Available Organoclays Studied by TGA-FTIR. *Thermochim. Acta* **2007**, *457*, 92−102.
(41) Xie, W.; Gao, Z.; Liu, K.; Pan, W.; Vaia, R.; Hunter, D.; Singh, A. Thermal Characterization of Organically Modified Montmorillonite. *Thermochim. Acta* **2001**, *367*−*368*, 339−350.
(42) Xie, W.; Gao, Z.; Pan, W.; Hunter, D.; Singh, A.; Vaia, R. Thermal Degradation Chemistry of Alkyl Quaternary Ammonium Montmorillonite. *Chem. Mater.* **2001**, *13*, 2979−2990.
(43) Saikia, B. J.; Parthasarathy, G. Fourier Transform Infrared Spectroscopic Characterization of Kaolinite from Assam and Meghalay, Northeastern India. *J. Mod. Phys.* **2010**, *1*, 206−210.
(44) Bishop, J.; Madejova, J.; Komadel, P.; Froschl, H. The Influence of Structural, Fe, Al, and Mg on the Infrared OH Bands in Spectra Dioctahedral Smectites. *Clay Miner.* **2002**, *37*, 607−616.
(45) Pavan, C.; Tomatis, M.; Ghiazza, M.; Rabolli, V.; Bolis, V.; Lison, D.; Fubini, B. In Search of the Chemical Basis of the Hemolytic Potential of Silicas. *Chem. Res. Toxicol.* **2013**, *26*, 1188−1198.
(46) Xi, Y.; Ding, Z.; He, H.; Frost, R. L. Structure of Organoclays-an X-ray Diffraction and Thermogravimetric Analysis Study. *J. Colloid Interface Sci.* **2004**, *277*, 116−120.
(47) Muller, K. H.; Motskin, M.; Philpott, A. J.; Routh, A. F.; Shanahan, C. M.; Duer, M. J.; Skepper, J. N. The Effect of Particle Agglomeration on the Formation of a Surface-connected Compartment Induced by Hydroxyapatite Nanoparticles in Human Monocyte-derived Macrophages. *Biomaterials* **2014**, *35* (3), 1074−88.
(48) Ruge, C. A.; Schaefer, U. F.; Herrmann, J.; Kirch, J.; Canadas, O.; Echaide, M.; Perez-Gil, J.; Casals, C.; Muller, R.; Lehr, C. The Interplay of Lung Surfactant Proteins and Lipids Assimilates the Macrophage Clearance of Nanoparticles. *PLoS One* **2012**, *7*, 1−10.
(49) Fan, Q.; Wang, Y. E.; Zhao, X.; Loo, J. S. C.; Zuo, Y. Y. Adverse Biophysical Effects of Hydroxyapatite Nanoparticles on Natural Pulmonary Surfactant. *ACS Nano* **2011**, *5*, 6410−6416.
(50) Lordan, S.; Higginbotham, C. L. Effect of Serum Concentration on the Cytotoxicity of Clay Particles. *Cell Biol. Int.* **2012**, *36*, 57−61.
(51) Zeinabad, H. A.; Zarrabian, A.; Saboury, A. A.; Alizadeh, A. M.; Falahati, M. Interaction of Single and Multi Wall Carbon Nanotubes with the Biological Systems: Tau Protein and PC12 Cells as Targets. *Sci. Rep.* **2016**, *6*, 1−21.
(52) Shannahan, J. H.; Brown, J. M.; Chen, R.; Ke, P. C.; Lai, X.; Mitra, S.; Witzmann, F. A. Comparison of Nanotube-Protein Corona Composition in Cell Culture Media. *Small* **2013**, *9*, 2171−2181.
(53) Rahman, M.; Laurent, S.; Tawil, N.; Yahia, L. H.; Mahmoudi, M. *Springer Ser. Biophys.* **2013**, *15*, 21−44.
(54) Saptarshi, S. R.; Duschl, A.; Lopata, A. L. Interaction of Nanoparticles with Proteins: Relation to Bio-reactivity of the Nanoparticle. *J. Nanobiotechnol.* **2013**, *11*, 1−12.
(55) Moore, T. L.; Rodriguez-Lorenzo, L.; Hirsch, V.; Balog, S.; Urban, D.; Jud, C.; Rothen-Rutishauser, B.; Lattuada, M.; Petri-Fink, A. Nanoparticle Colloidal Stability in Cell Culture Media and Impact on Cellular Interactions. *Chem. Soc. Rev.* **2015**, *44*, 6287−6305.
(56) Loosli, F.; Vitorazi, L.; Berret, J.; Stoll, S. Towards a Better Understanding on Agglomeration Mechanisms and Thermodynamic Properties of TiO2 Nanoparticles Interacting with Natural Organic Matter. *Water Res.* **2015**, *80*, 139−148.
(57) Sauer, U. G.; Aumann, A.; Ma-Hock, L.; Landsiedel, R.; Wohlleben, W. Influence of Dispersive Agent on Nanomaterial Agglomeration and Implications for Biological Effects in vivo or in vitro. *Toxicol. In Vitro* **2015**, *29* (1), 182−186.
(58) Hubbs, A.; Greskevitch, M.; Kuempel, E.; Suarez, F.; Toraason, M. Abrasive Blasting Agents: Designing Studies to Evaluate Relative Risk. *J. Toxicol. Environ. Health, Part A* **2005**, *68*, 999−1016.
(59) Yang, A.; Cardona, D. L.; Barile, F. A. In vitro Cytotoxicity Testing with Fluorescence-based Assays in Cultured Human Lung and Dermal Cells. *Cell Biol. Toxicol.* **2002**, *18*, 97−108.
(60) Farcal, L.; Torres Andon, F.; Di Cristo, L.; Rotoli, B. M.; Bussolati, O.; Bergamaschi, E.; Mech, A.; Hartmann, N. B.; Rasmussen, K.; Riego-Sintes, J.; Ponti, J.; Kinsner-Ovaskainen, A.; Rossi, F.; Oomen, A.; Bos, P.; Chen, R.; Bai, R.; Chen, C.; Rocks, L.; Fulton, N.; Ross, B.; Hutchison, G.; Tran, L.; Mues, S.; Ossig, R.; Schnekenburger, J.; Campagnolo, L.; Vecchione, L.; Pietroiusti, A.; Fadeel, B. Comprehensive In Vitro Toxicity Testing of a Panel of Representative Oxide Nanomaterials: First Steps towards an Intelligent Testing Strategy. *PLoS One* **2015**, *10* (5), e0127174.
(61) Das, S.; Singh, S.; Singh, V.; Joung, D.; Dowding, J. M.; Reid, D.; Anderson, J.; Zhai, L.; Khondaker, S. I.; Self, W. T.; Seal, S. Oxygenated Functional Group Density on Graphene Oxide: Its Effect on Cell Toxicity. *Part. Part. Syst. Charact.* **2013**, *30* (2), 148−157.
(62) Zhang, H.; Dunphy, D. R.; Jiang, X.; Meng, H.; Sun, B.; Tarn, D.; Xue, M.; Wang, X.; Lin, S.; Ji, Z.; Li, R.; Garcia, F. L.; Yang, J.; Kirk, M. L.; Xia, T.; Zink, J. I.; Nel, A.; Brinker, C. J. Processing Pathway Dependence of Amorphous Silica Nanoparticle Toxicity: Colloidal vs Pyrolytic. *J. Am. Chem. Soc.* **2012**, *134* (38), 15790−804.
(63) Tarn, D.; Ashley, C. E.; Xue, M.; Carnes, E. C.; Zink, J. I.; Brinker, C. J. Mesoporous Silica Nanoparticle Nanocarriers: Biofunctionality and Biocompatibility. *Acc. Chem. Res.* **2013**, *46*, 792−801.
(64) Ray, P. D.; Huang, B. W.; Tsuji, Y. Reactive Oxygen Species (ROS) Homeostasis and Redox Regulation in Cellular Signaling. *Cell. Signalling* **2012**, *24* (5), 981−90.
(65) Sterman, S.; Marsden, J. G. Silane Coupling Agents. *Ind. Eng. Chem.* **1966**, *58*, 33−37.
(66) Soteropulos, C. E.; Hunt, H. K. Attaching Biological Probes to Silica Optical Biosensors Using Silane Coupling Agents. *J. Visualized Exp.* **2012**, *63*, e3866.
(67) Ojea-Jimenez, I.; Urban, P.; Barahona, F.; Pedroni, M.; Capomaccio, R.; Ceccone, G.; Kinsner-Ovaskainen, A.; Rossi, F.; Gilliland, D. Highly Flexible Platform for Tuning Surface Properties of Silica Nanoparticles and Monitoring Their Biological Interaction. *ACS Appl. Mater. Interfaces* **2016**, *8* (7), 4838−4850.
(68) Meczynska-Wielgosz, S.; Piotrowska, A.; Majkowska-Pilip, A.; Bilewicz, A.; Kruszewski, M. Effect of Surface Functionalization on the Cellular Uptake and Toxicity of Nanozeolite A. *Nanoscale Res. Lett.* **2016**, *11* (1), 1−14.
(69) Ibarguren, M.; Lopez, D. J.; Escriba, P. V. The Effect of Natural and Synthetic Fatty Acids on Membrane Structure, Microdomain Organization, Cellular Functions and Human Health. *Biochim. Biophys. Acta, Biomembr.* **2014**, *1838* (6), 1518−1528.
(70) Papanikolaou, G.; Pantopoulos, K. Iron Metabolism and Toxicity. *Toxicol. Appl. Pharmacol.* **2005**, *202* (2), 199−211.
(71) Eaton, J. W.; Qian, M. Molecular Basis of Cellular Iron Toxicity. *Free Radical Biol. Med.* **2002**, *32*, 833−840.
(72) Breznan, D.; Das, D. D.; O'Brien, J. S.; MacKinnon-Roy, C.; Nimesh, S.; Vuong, N. Q.; Bernatchez, S.; DeSilva, N.; Hill, M.; Kumarathasan, P.; Vincent, R. Differential Cytotoxic and Inflammatory Potency of Amorphous Silicon Dioxide Nanoparticles of Similar Size in Multiple Cell Lines. *Nanotoxicology* **2017**, *11*, 223−235.
(73) Wallace, W. E.; Keane, M. J.; Murray, D. K.; Chisholm, W. P.; Maynard, A. D.; Ong, T. Phosopholipid Lung Surfacant and Nanoparticle Surface Toxicity: Lessons from Diesel Soots and Silicate Dusts. *J. Nanopart. Res.* **2006**, *9*, 23−38.
(74) Napierska, D.; Thomassen, L. C. J.; Rabolli, V.; Lison, D.; Gonzalez, L.; Kirsch-Volders, M.; Martens, J. A.; Hoet, P. H. Size-Dependent Cytotoxicity of Monodisperse Silica Nanoparticles in Human Endothelial Cells. *Small* **2009**, *5*, 846−853.
(75) Lin, Y.; Haynes, C. L. Impacts of Mesoporous Silica Nanoparticle Size, Pore Ordering, and Pore Integrty on Hemolytic Activity. *J. Am. Chem. Soc.* **2010**, *132*, 4834−4842.
(76) Re, F.; Zanetti, A.; Sironi, M.; Polentarutti, N.; Lanfrancone, L.; Dejana, E.; Colotta, F. Inhibition of Anchorage-dependent Cell Spreading Triggers Apoptosis in Cultured Human Endothelial Cells. *J. Cell Biol.* **1994**, *127*, 537−546.

DOI: 10.1021/acsami.7b06657
ACS Appl. Mater. Interfaces 2017, 9, 32323−32335

(77) Frisch, S. M.; Francis, H. Disruption of Epithelial Cell-Matrix Interactions Induces Apoptosis. *J. Cell Biol.* **1994**, *124* (4), 619−626.
(78) Snyder, R. J.; Hussain, S.; Rice, A. B.; Garantziotis, S. Multiwalled Carbon Nanotubes Induce Altered Morphology and Loss of Barrier Function in Human Bronchial Epithelium at Noncytotoxic Doses. *Int. J. Nanomed.* **2014**, *9*, 4093−4105.
(79) Dong, C.; Kashon, M. L.; Lowry, D. T.; Dordick, J. S.; Reynolds, S. H.; Rojanasakul, Y.; Sargent, L. M.; Dinu, C. Z. Exposure to Carbon Nanotubes Leads to Changes in the Cellular Biomechanics. *Adv. Healthcare Mater.* **2013**, *2*, 1−7.
(80) Zhou, X.; Wang, B.; Chen, Y.; Mao, Z.; Gao, C. Uptake of Cerium Oxide Nanoparticles and Their Influences on Functions of A549 Cells. *J. Nanosci. Nanotechnol.* **2013**, *13*, 204−215.
(81) Tarantola, M.; Pietuch, A.; Schneider, D.; Rother, J.; Sunnick, E.; Rosman, C.; Pierrat, S.; Sonnichsen, C.; Wegener, J.; Janshoff, A. Toxicity of Gold-nanoparticles: Synergistic Effects of Shape and Surface Functionalization on Micromotility of Epithelial Cells. *Nanotoxicology* **2011**, *5* (2), 254−268.
(82) Xia, T.; Kovochich, M.; Liong, M.; Madler, L.; Gilbert, B.; Shi, H.; Yeh, J. I.; Zink, J. I.; Nel, A. E. Comparison of the Mechanism of Toxicity of Zinc Oxide and Cerium Oxide Nanoparticles Based on Dissolution and Oxidative Stress Properties. *ACS Nano* **2008**, *2* (10), 2121−2134.
(83) Maisanaba, S.; Puerto, M.; Pichardo, S.; Jorda, M.; Moreno, F. J.; Aucejo, S.; Jos, A. In vitro Toxicological Assessment of Clays for Their Use in Food Packaging Application. *Food Chem. Toxicol.* **2013**, *57*, 266−275.

DOI: 10.1021/acsami.7b06657
ACS Appl. Mater. Interfaces 2017, 9, 32323−32335